Solid Freeform Fabrication 2022: Proceedings of the 33rd Annual International Solid Freeform Fabrication Symposium – An Additive Manufacturing Conference
Reviewed Paper

LASER LINE PROFILE SCANNING FOR POWDER BED TOPOGRAPHY MEASUREMENT

Jaime Berez*, Christopher Saldaña*

*George W. Woodruff School of Mechanical Engineering, Georgia Institute of Technology, Atlanta, GA 30332

Abstract

The metal additive manufacturing (AM) method of laser powder bed fusion (LPBF) relies upon the formation of uniform, densely packed, and defect free powder layers. The direct measurement of as-spread powder layer quality is challenging owing to the fine size of the powder bed features and limited selection of instruments which can assess the powder bed in-situ. This work assesses the fitness of a laser line profiling instrument in the topographical measurement of an LPBF system powder bed. Firstly, results which assess the minimum resolvable feature size are presented, which suggest the instrument can capture microscopic powder bed defects. The ability of the instrument to detect macroscopic powder bed defects is also shown. Measures of bed quality, based on areal surface texture analysis, are explored for their potential as process signals.

Keywords: laser powder bed fusion (LPBF), powder bed measurement, topography, laser line profiler, surface texture

Introduction

In-situ monitoring of metal additive manufacturing (AM) and laser powder bed fusion (LPBF) processes have been shown to provide rich data sets which may be leveraged to capture out-of-control process behavior and relate processing anomalies to workpiece defects [1,2]. Of the many candidate process signals which may be measured [1], measurement of the as-spread powder bed has received somewhat less attention but could offer significant insights into the LPBF manufacturing process and its outcomes. Powder bed quality, i.e., low packing and lack of uniformity, is an understudied process behavior in LPBF which may cause significant lack-of-fusion (LoF) porosity – the absence of material fusion due to poor melt pool overlap [3,4]. Such porosity is concerning due to it's well-known impacts on workpiece mechanical properties [5].

Powder bed defects may be considered micro- or macroscopic, as classified in the this work. Microscopic defects include small voids in the bed due to low powder packing or the localized excess of feedstock material due to large or agglomerated powder and spatter particles. Both defects may contribute to LoF in the workpiece due to too little feedstock material or too much to be fully melted. Literature reviews [4] have shown that powder packing has largely been studied via simulations, not experimentation. A small number of studies [5–8] have suspected in-operando contamination of the powder bed by spatter to produce LoF defects which drive poor mechanical performance. These claims have been largely circumstantial and require direct analysis of the powder bed to support them. Macroscopic powder bed effects include spreading defects owing to the physical interaction of the recoating mechanism with the powder bed. Recoater edge damage or vibration can produce defects such as streaking [9–11], or hopping [10–12], but this

has generally been observed optically or via simulation. A source of ground truth for these defects, in the form of powder bed topography, is missing.

There is a further need for powder bed measurement technology due to current deficiencies in the ability to quantify and control powder 'spreadability'. There is a lack of AM-specific standardized powder testing techniques [13,14], frequent low uniformity between powder lots [15,16], uncontrolled evolution in powder properties due to environment/recycling/reconditioning [17–21], and poor correlation between powder quality metrics and LPBF process suitability, i.e., spreadability [13,22]. As such, LPBF practitioners often rely upon operator expertise, rather than quantifiable and systematic measures to identify powders with poor spreadability.

A flexible, practical, and well-qualified method capable of measuring powder bed quality as a process signal is required to assess its contributions to the overall LPBF process. Prior work has captured spatter redistribution onto the powder bed via high spatial resolution imaging in an interrupted build process [23]. Results showed that spatter can gather in downstream regions of the build area and vary in its concentration as a function of upstream scan pattern directionality. Other efforts have used optical imaging to identify "contaminated powder," "debris" and the aforementioned macroscopic spreading defects either through human evaluation of images or [9] classification via machine learning approaches [10,11]. Some early efforts have explored sensing methods capable of in-situ powder bed topography measurement. Methods such as X-ray imaging of the bed thickness [24] and fringe projection [25,26] have been explored, but they are limited due to experimental complexity. Laser line profile scanning has been demonstrated in polymer powder bed systems [27] and similar methods directed at as-fused workpiecetopography detection have been used in LPBF systems [28]. Ref. [27] provided some proposed measures of powder bed quality, but further work is needed.

Laser line profiling is an attractive approach to powder bed measurement due to its relatively good spatial resolution and high data throughput. However, topographical measurement of a powder bed via such a method is a complex measurement task in need of qualification. The present work seeks to explore this sensing modality and its suitability for the measurement task. Measurement capabilities are baselined, powder bed scans are presented to demonstrate the results of on-machine sensing, and powder bed quality analysis methods are explored.

Materials and Methods

A *Keyence LJ-X8080* laser line profiler, depicted in Figure 1(a), was evaluated for its fitness for the powder bed measurement task. This instrument projects a 405 nm blue LED laser line onto the workpiece surface. A high-resolution CMOS sensor, situated to have an oblique view of the line profile as projected onto the workpiece, measures the line shape at 3200 points with 12.5 μm sampling interval (instrument *X* direction). The workpiece surface height (instrument *Z* direction) is calculated via triangulation, producing data with a 12.5 μm digitization step in a range of ±20.5 mm from its reference working distance of 73 mm. The instrument manufacturer reported repeatability is 0.5 and 3 μm in the *X* and *Z* directions, respectively. Linearity in the *Z* direction is reported as ±0.03 of the full-scale range (41 mm). Through high frequency imaging of the line profile in combination with translation of the instrument relative to the workpiece in the *Y* direction (mutually perpendicular *X* and *Z* directions) 3D data sets can be produced, i.e., areal height maps.

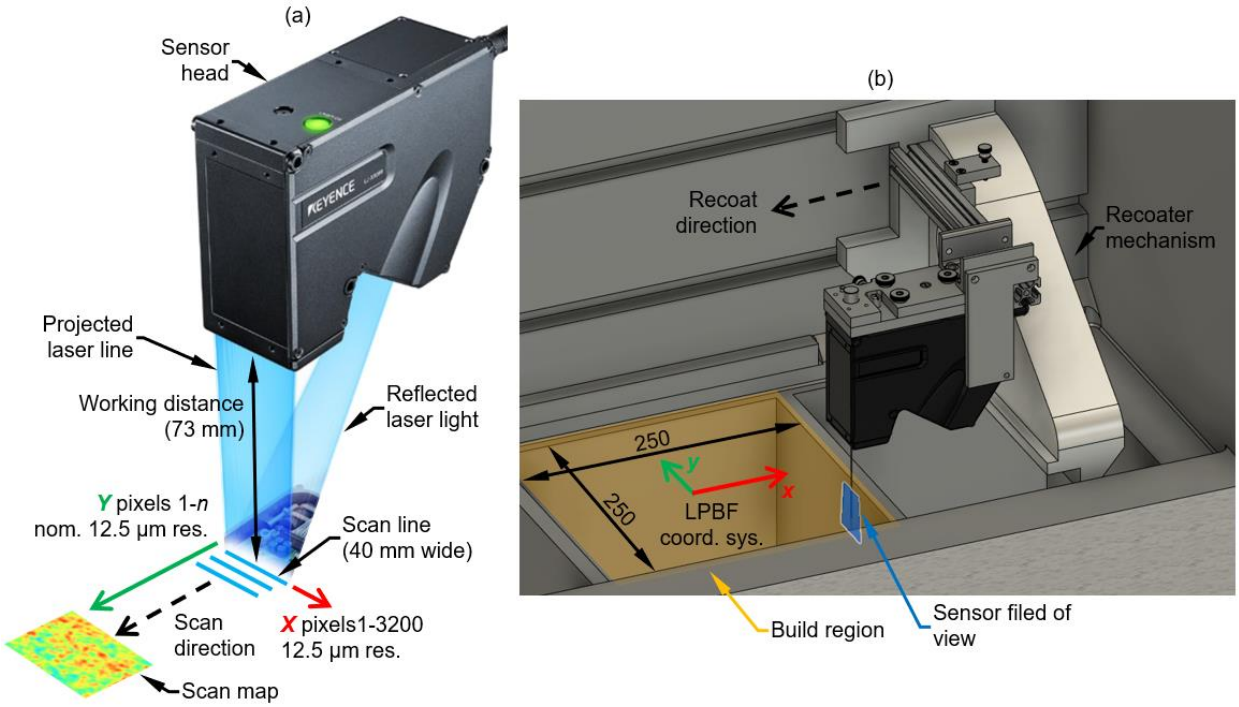

Figure 1. (a) Instrument schematic and description (figure adapted from Keyence Corporation). (b) Instrument as implemented in an EOS M280 LPBF system. All dimensions shown are in mm.

To acquire measurements of the LPBF system powder bed, the scanner was fixtured to the recoating mechanism, as seen in Figure 1(b), orienting the laser line projection direction nominally orthogonal to the powder bed. As such, the acquired *Z* data directly corresponded to powder bed height. The recoater was translated at a nominal speed of 40 mm/s during data acquisition and line profiles were acquired at 3200 Hz, thereby producing a nominal spacing between scan lines, i.e., *Y* sampling interval, of 12.5 µm. Note that the LPBF system coordinate *X* and *Y* directions as seen in Figure 1(b) and consistent with convention as per ISO/ASTM-52912-13 are different than that of the instrument, as seen in Figure 1(a). All data was exported as height data (*Z*) over a 3200 x *n* (*X* points x *Y* points) grid without filtering, interpolation, or other corrections. Data was processed in *MATLAB R2021b* using code developed by the authors.

Data was analyzed as follows, in a manner consistent with methodology and terminology of ISO 25178-2:2012. The reconstructed areal height map was treated as the primary surface, S, where the native resolution of the instrument applied an S-filter to the raw data. An F-operation was applied to remove the nominal form of the workpiece surface by subtracting a plane of best fit, calculated via linear least-squares. This formed the S-F surface, i.e., the scale-limited surface. The plane of best fit defines the reference surface, depicted as the $z = 0$ plane in subsequent figures.

Powder beds formed on an *EOS M280* commercial LPBF system were measured. The recoating mechanism traversed a recoater blade over a 250 x 250 mm build region. Two recoating blades, available from the LPBF system OEM, were studied – a 'soft' brush recoater blade and 'hard' high speed steel (HSS) recoater blade, each having a nominally straight edge slightly longer than 250 mm wide build region. The powder used in this study was supplied by *Kennametal* under the commercial product name of *Delcrome 316L* and had a nominal powder size distribution (PSD) ranging from 10 to 45 µm. The powder was spread and measured in its virgin state.

Instrument characterization

To fully qualify laser line profile scanning as a method for powder bed measurement there are numerous metrological characteristics to assess. ISO 25178-600 provides an expansive list of characteristics for topology measurement methods, but a complete qualification effort is out of the scope of the present work. This study focused on qualification of topographic spatial resolution is focused on. This characteristic is chiefly important as it indicates the ability of the instrument to distinguish "closely spaced surface features," such as those typical to a powder bed. Important powder bed features may include the typical individual powder particle (10 to 45 µm), spatter particles (>100 µm), and powder bed voids which can create concerning lack of fusion defects (>100 µm). The sampling intervals and digitization steps of the instrument (12.5 µm in the *X*, *Y*, and *Z* directions) nears the size of these features. As such, the present study has undertaken a preliminary investigation of the laser line profile scanner's ability to resolve closely spaced features on this size scale, i.e., topographic spatial resolution.

A measurement article was manufactured with discrete, individually measurable features intended to mimic typical microscopic features sizes in the powder bed. Figure 2(a) shows the design of an isogrid unit of conical holes that could be patterned to form larger hole arrays. An article was manufactured in 360 brass by milling a flat surface, polishing the surface with fine grit sand paper, and drilling conical holes using a drill bit with a tip included angle of 60° and flat bottom of Ø0.100 mm. Multiple hole arrays were manufactured with distinct feature sizes and spacings intended to assess topographic spatial resolution. Figure 1(b-d) show measurements of hole arrays with varying features sizes acquired with a *Keyence VR-6200* optical profiler – a relatively high-resolution bench-top instrument used to produce reference measurements for this study. The holes in these arrays were assessed to have the dimensions d = 0.132 mm (conical hole truncated diameter), d_b = Ø0.100 mm (flat bottom diameter), and a = 60° (included angle), and varying spacings of l_g = (b) 0.200, (c) 0.220, and (d) 0.240mm. As is apparent, the depth relative to the artifact top face is approximately 0.020 mm.

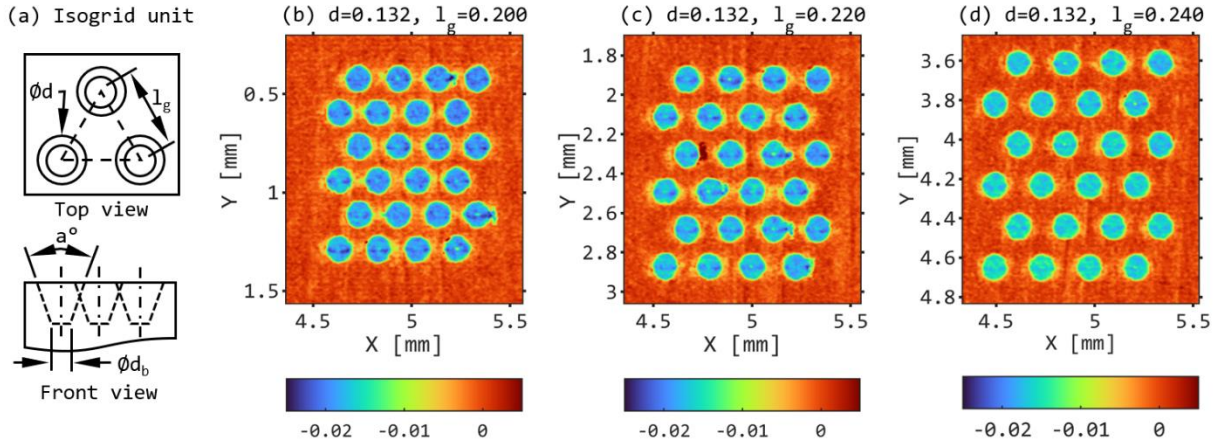

Figure 2. (a) Isogrid unit used in article design. (b-d) Optical profiler data of hole arrays with varying feature sizes. Z data is in [mm].

Figure 3 shows the same three hole arrays as in Figure 4, but measured with the on-LPBF system laser line profiler. The scans of each hole array show the ability of the instrument to resolve the progressively reduced space between holes, ranging from approximately (a) 0.070, to (b) 0.090,

to (c) 0.110 mm. As can be seen in Figure 3(a), at the smallest spacing of 0.070 mm, the area between holes is only represented by small grouping of pixels which are bridged slightly at the closest points between holes. In Figure 3(b) and (c) this condition improves somewhat, with almost no examples of bridging between holes. Notably, in for all hole spacings, the holes themselves appear to show several pixels in their middle which indicate peak-like geometry within the hole. The cause for this measurement artifact is unclear, and further investigation is warranted. Overall, the results are encouraging – the measurement method can assess the presence of small and shallow negative features, i.e., the 0.132 mm diameter 0.020 mm deep conical holes, and it also achieves a topographical spatial resolution of approximately 0.080-0.100 mm. These preliminary results suggest the measurement method to be suitable for the detection of similarly sized microscopic features in the powder bed.

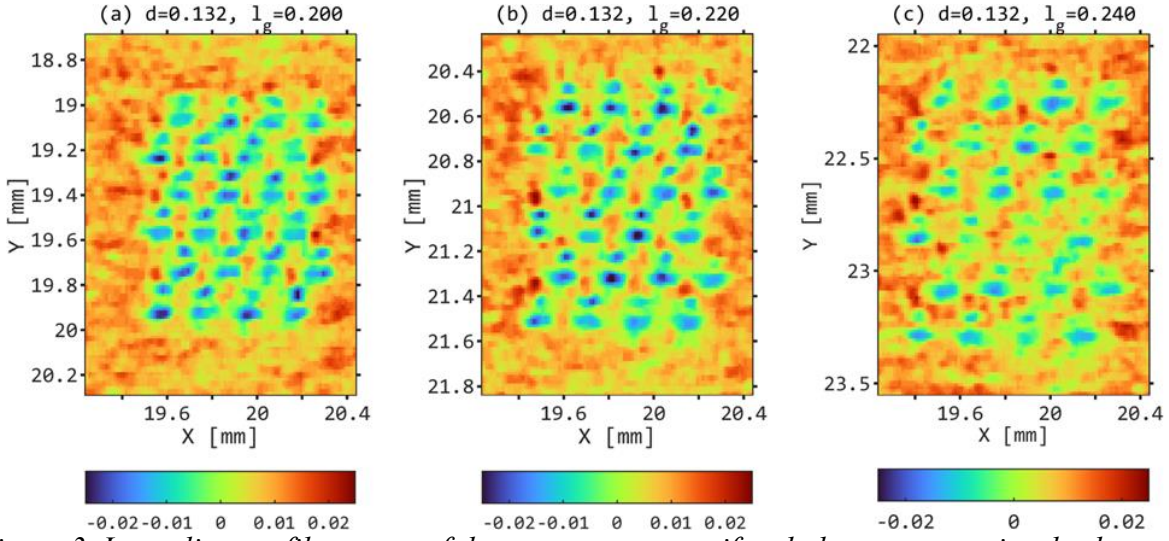

Figure 3. Laser line profiler scans of the measurement artifact hole arrays previously shown in Figure 2(b-d). Z data is in [mm].

Powder bed measurements

This section shows the results of powder bed measurements using the laser line profiler. Areal height maps were produced by measuring 4000 lines as the instrument was translated in the recoater direction, using the parameters earlier described. As such, areal maps were approximately 40 x 50 mm in area. Note that data from the powder bed surface was not returned at the $\pm X$ edges of the laser line. This is expected due the working distance of the instrument producing a cropped field of view for the sensor. Subsequent figures show areal height maps which are scale-limited surfaces, having been subject to an S-filter and F-operation as earlier defined.

Figure 4 shows a height map of a powder bed spread using a brush recoater blade. Brush recoaters and other 'soft' recoaters are popular for their ability to accommodate interference and physical interaction with the fused workpiece within the powder bed. Even so, by nature, soft recoaters are prone to damage. In particular, the examined brush recoater has an edge which is only as straight as the bristles which form it can be. As such, streaks are formed on the powder bed. For example, the streak formed between the approximate X values of 17 and 19 mm is up to 0.080 mm taller than the average powder bed height in this height map. This value is similar to or

greater than the depth of a melt pool in the LPBF process and could lead to planar LoF on a layer-wise basis in this area. Far thinner streaks are visible throughout the height map, likely formed due to individual or small groups of bristles having slightly different lengths than their neighbors. This data shows the promise of the sensing method for assessing the damage state of a soft recoater with quantitative evidence, as opposed to subjective operator judgement.

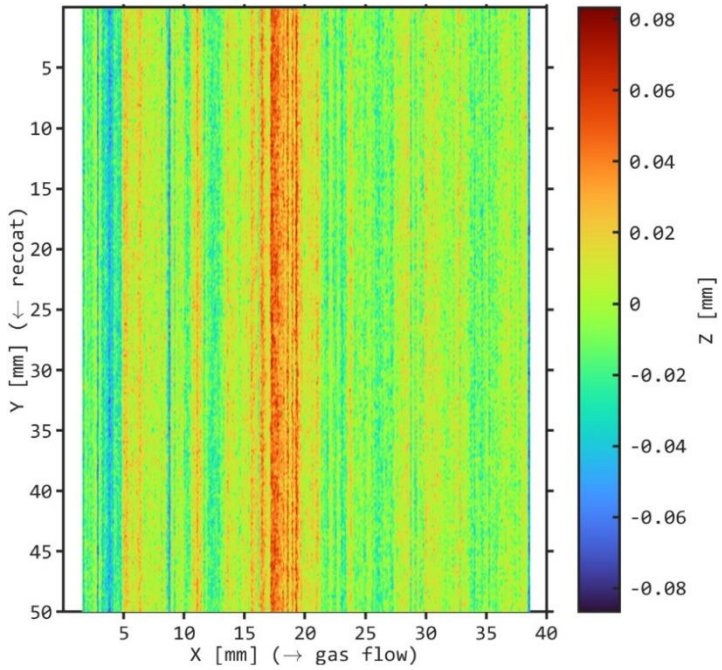

Figure 4. Powder bed spread with a brush recoater blade.

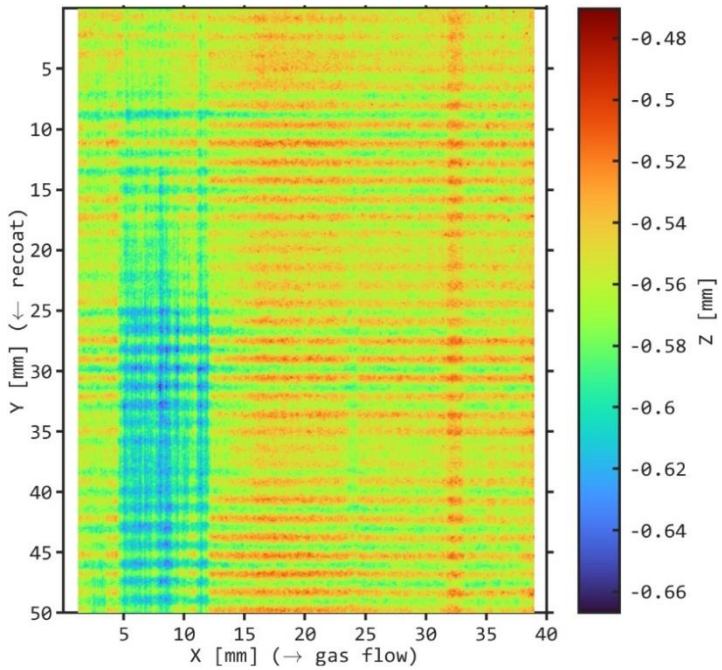

Figure 5. Powder bed spread with a HSS recoater blade. Total bed thickness was 0.2 mm.

Figure 5 shows a height map of a powder bed which was approximately 0.2 mm in total bed thickness, spread with a HSS recoater blade over a steel build plate with a ground finish. The data shows elongated peaks and valleys in a periodic pattern, oriented perpendicular to the to the recoat direction, i.e., along the edge of the translating recoater blade. This is mostly likely an artifact of recoater hopping, possibly resulting from the high shear and normal forces generated in the thin powder bed. Notably, this phenomenon was difficult for the LPBF system operator to distinguish using visual cues, and its nature was unclear without the height map data. The authors are unaware of other experimental data which has shown this effect interms of quantitative topography.

Figure 6 shows a powder bed spread with a HSS recoater, approximately 0.8 mm in total bed thickness. This powder bed appears to have relatively few macroscopic defects, such as the earlier displayed streaking and hopping. There does appear to be one major streak, in addition some more minor ones, located between the approximate X values of 20 and 23 mm. The streak is up to 0.049 mm taller than the average powder bed height in this scan. The LPBF system operator notably did not observe this defect from visual cues, indicating again that the quantifiable height map data from the instrument produces valuable insight into the damage state of a recoater blade.

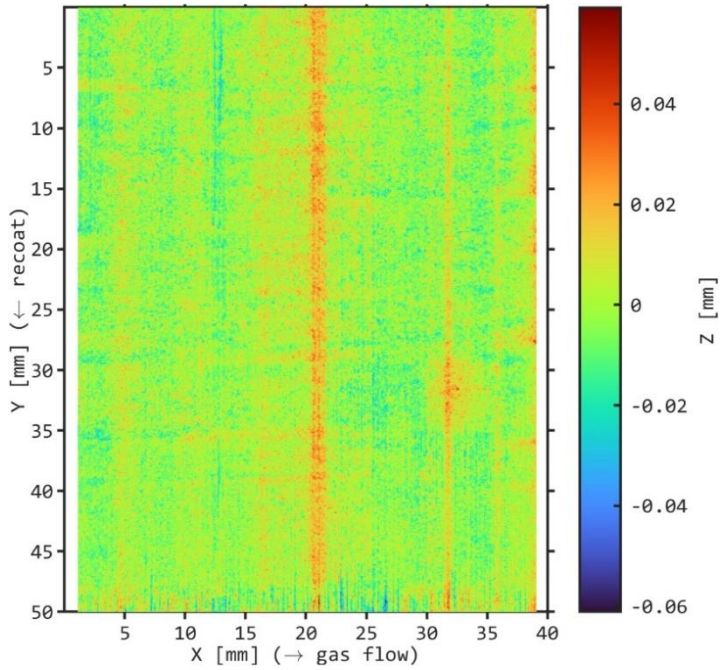

Figure 6. Powder bed spread with a HSS recoater blade. Total bed thickness was 0.8 mm.

Figure 7 shows a detail view of the data previously displayed in Figure 6. The topography does not clearly show individual powder particle hemispherical geometry, but this is not expected due to the scan resolution. Nonetheless, Figure 7 shows the potential of the examined instrument to identify microscopic powder bed defects, such as local low density, individual voids in the bed, or contamination by large spatter particles. Note that the LPBF process was not performed during measurement of the powder beds presented here, so there is no possibility of spatter contamination in these cases. Even so, some individual peaks and valleys appear in the scan, which illustrate potential microscopic defects in the powder bed. The earlier presented topographical spatial

resolution characterization affirms that the data in Figure 7 is not solely noise – the instrument has the capability to distinguish the features sizes which appear in this data set.

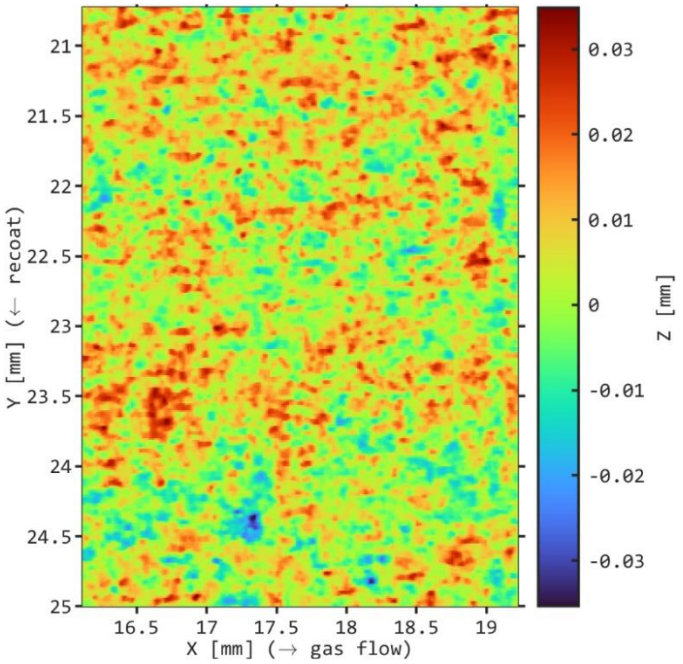

Figure 7. Local region of the powder bed data shown in Figure 6.

Powder bed measurement analysis

While the above affirms the ability of the laser line profiler instrument to detect both macroscopic and microscopic defects through human-based inspection of the data sets, an algorithmic method is preferable. The field of areal surface texture analysis offers several potential data analysis techniques which are of interest for this task. Terminology consistent with ISO 25178-2:2012 is used here, where possible. Consider a small region of interest similar to that in Figure 7, i.e., an evaluation area, which can be analyzed for defect content. A wide variety of areal surface texture field parameters can be calculated, each of which summarize the data into a single numerical quantity. In this work nine parameters have been selected for analysis. The first five are known as amplitude parameters: Sa (arithmetic average), Sq (root mean square), Sz (total height variation), Ssk (skewness), and Sku (kurtosis). These parameters summarize the height data in an areal surface texture data set when said data is treated as a distribution of discrete height values, i.e., the height density curve. The other four parameters are known as functional parameters and are derived the height data when treated as the inverse of its empirical cumulative density function form, i.e., the material ratio curve. These four parameters are Vmp (peak material volume), Vmc (core material volume), Vvc (core void volume), and Vvv (valley void volume). A summary of the mathematical definitions of these parameters can be found in ISO 25178-2:2012.

An intuitive analysis of each parameter provides reasoning for their selection. Sa and Sq summarize the average spread in the data – high values indicate high roughness, i.e., many tall peaks and deep valleys and thus low powder bed uniformity. Sku provides a similar assessment, although it has the opposite response in value – low kurtosis indicates high spread. Ssk detects nonsymmetric height density distributions, i.e., the presence of more peaks than valleys or visa

versa. The functional parameters are all direct indications of the volume between two cutoff planes respective to the surface. Vmp is a measure of the volume under surface peaks up to the height value corresponding to 10% on the material ratio curve. This might detect spatter, streaking, or other similar anomalous features. Vmc and Vvc measure the volume of material and void between the heights corresponding to the 10% and 80% material ratio values. Vvv measures the volume between the height value corresponding to the 80% material ratio value and all valleys under this value. This might be an indication of valley-like streaking, low powder bed density, etc.

To test the suitability of these metrics as process signals for local powder bed quality, a sample region of a scanned powder bed was analyzed. Figure 8(a) and Figure 9(a) both show a 3 x 35 mm (X x Y) region of the powder bed measurement data previously shown in Figure 6. Evaluation areas 3 x 3 mm (X x Y) in size were tiled over the region in (a), beginning at (x, y) = (2, 5) and incrementing in x value by 3 mm up to (x, y) = (35, 5). In the case of Figure 8, parameters were calculated directly on the evaluation regions, with an F-operation having been performed prior on the entire 40 x 50 mm scan. In Figure 9, each evaluation area was individually subject to an F-operation, which subtracted the plane of best fit from the data prior to parameter calculation. In both figures, the calculated amplitude and functional parameters are shown in sub-figures (b) and (c), respectively. All parameter values were normalized so that they may be plotted on the same axes. If P_i is the parameter for an evaluation region I and $\boldsymbol{P}$ is the set of a parameters of all evaluation areas, the normalized parameters N_i were calculated as $N_i = \frac{P_i - \min(P)}{\max(P) - \min(P)}$.

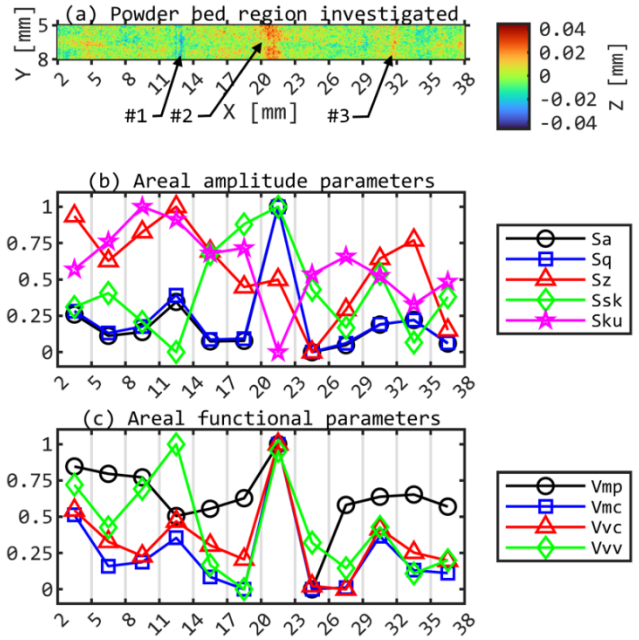

Figure 8. (a) Investigated powder bed region. (a) amplitude and (b) functional parameters on normalized scales, evaluated over localized 3x3 mm evaluation areas spanning the data in (a). Only the originating 40x50 mm areal height map was subject to an F-operation.

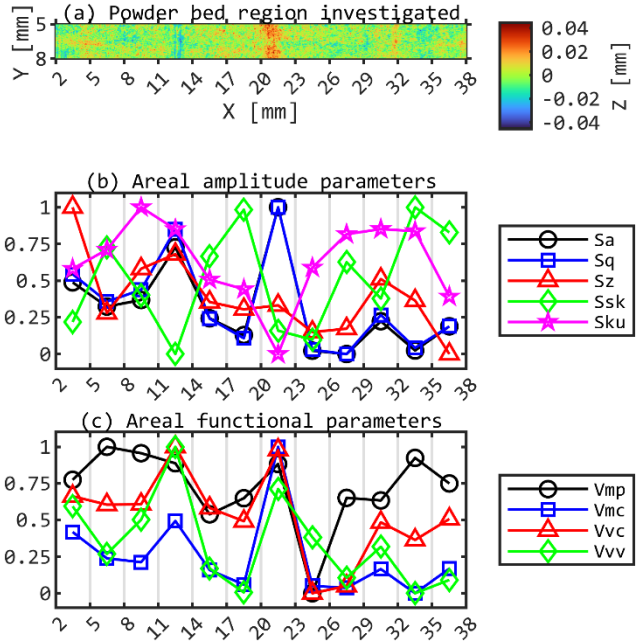

Figure 9. (a) Investigated powder bed region. (a) amplitude and (b) functional parameters on normalized scales, evaluated over localized 3x3 mm evaluation areas spanning the data in (a). Each evaluation area was subject to an individual F-operation.

Visual inspection of the investigated region shown in Figure 8(a) and Figure 9(a) shows that there are defects in the evaluation areas with *X* bounds of 11-14, 20-23, and 29-32 mm, labeled defects #1, #2, and #3, respectively. Defect #1 is part of a minor valley-like streak, #2 part of a large and severe peak-like streak, and #3 part of a minor peak-like streak. Sa and Sq trend closely together, and each appear to show a high normalized value for defects #1 and #2. When the parameters are evaluated without an F-operation on the evaluation region (Figure 8) the non-anomalous regions appear to show a more consistent value, whereas when the evaluation region is subject to an individual F-operation (Figure 9) the data does not appear to have a baseline value. Ssk shows even more severe differences depending on use of an F-operation. When the no F-operation is performed on the evaluation region (Figure 8), Ssk has its lowest value corresponding to the valley-like defect #1 and highest corresponding to the peak-like defect #2. It also spikes slightly for the minor peak-like defect #3. When F-operations are locally applied (Figure 9), Ssk shows no clear pattern corresponding to the visual identification of powder bed defects. Note that Ssk, before normalization, ranges from -1 to 1, where a negative value indicates right skewness and positive indicates left skewness. Within this context it is clear that using a globally applied F-operator allows Ssk to detect if a local analysis region is biased towards a thick or thin powder bed. Sku shows a low value for the peak-like streak but not many other trends while Sz does not provide any intuitive response to the data.

The functional parameters in sub-figure (c) of Figure 8 and Figure 9 also show some sensitivity to powder bed defects. The global application of an F-operator (Figure 9) results in all examined functional parameters having a high normalized value in the location of the peak-like defect #1. This is explained by the high surface roughness (high Sa and Sq) in this area which indicates high peaks and valleys which have correspondingly large, subtended volumes. Vvv is high in normalized value corresponding to both the valley- and peak-like defects #1 and #2. When the F-operation is locally applied to evaluation areas the same observations largely apply, except that Vvc now additionally spikes in normalized value for the less severe valley-like defect #3.

To further examine the suitability of these surface texture field parameters as signals for local powder bed quality, the areal height map shown in Figure 6 was more expansively analyzed. Sq, Ssk, Vmc, and Vvv were selected for closer analysis due to the prior observations of their strong response to defects. As described above, 3 x 3 mm evaluation areas were used, this time tiled over the *X* range of 2 to 38 mm and the *Y* range of 5 to 44 mm, excluding the edges of the areal height map. Figure 10 shows the selected parameters evaluated on a height map was subject to a global F-operator. This approach was selected as the prior observations showed it to produce more intuitive results in most cases. Each parameter the ability to identify the long, severe peak-like defect #2 over the measured powder bed. In addition, each highlights the presence of a local peak-like defect with the approximate coordinates of (x, y) = (30, 35), referring to Figure 6. Ssk has a very sensitive response to the relatively minor peak-like streak #3 in the x = 29-32 location, something Sq fails to identify. It also shows high values, i.e., positive skewness, in a large range from x = 14 to 23. Referring to Figure 6, this appears to correspond with a region skewed towards positive values not only due to the severe streak #3, but also to a lesser extent, in the surrounding region. Vmc is noteworthy for its similar ability to identify the minor peak-like streak #3, where values are slightly higher than the rest of the powder bed. Vvv identifies streak #2 and the peak at (x, y) = (30, 35). Additionally, it highlights a portion of streak #1 where it is most severe in the y = 0-10 region. Other parameters appeared to be less sensitive to this feature.

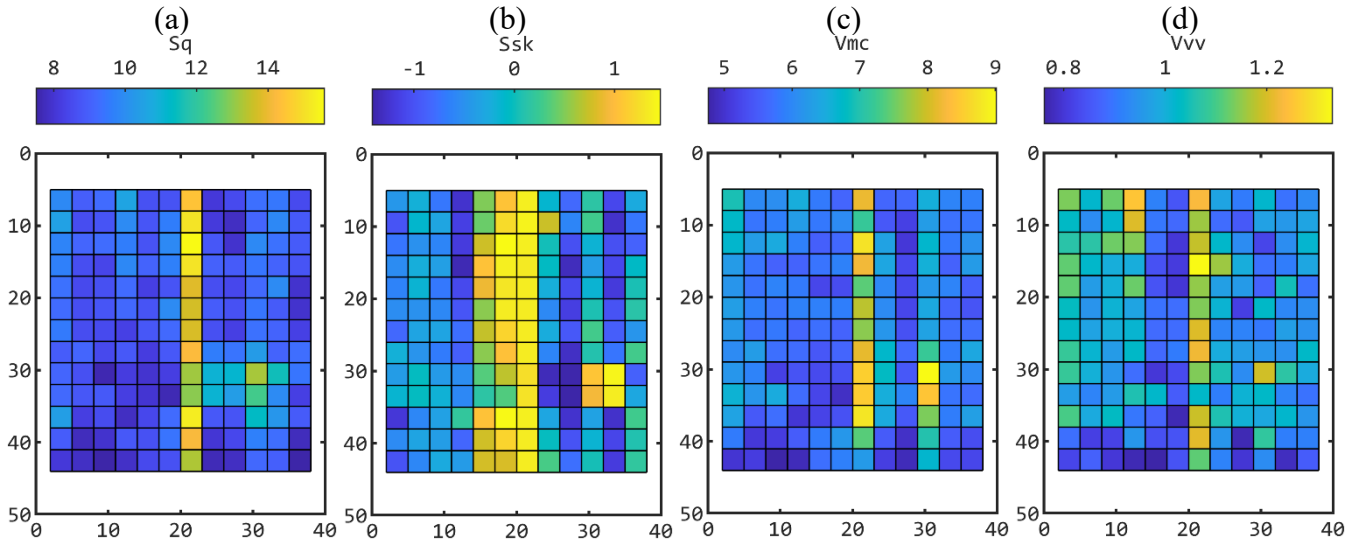

Figure 10. Areal surface texture parameters (a) Sq, (b) Ssk, (c) Vmc, (d) Vvv, calculated over 3 x 3 mm evaluation areas tiled over the areal height map shown in Figure 6. X and Y units are in mm. Amplitude parameters are in units of [µm]. Functional parameters are in units of [µm^3/mm].

Conclusions

Preliminary efforts to determine the metrological characteristics of laser line profile scanning for powder med measurement indicate its fitness for the task. Critically, the assessment of topographic spatial resolution through the measurement of powder bed like measurement article indicate the ability of the method to distinguish individual small features in the powder bed, on the order of 0.080-0.100 mm. Further characterization efforts will need to expand this work. Scaling error and linearity of the instrument *Y* axis, which is subject to error from off-nominal recoater mechanism velocity, should be studied. Similarly, a characterization of flatness deviation would assess how the straightness in travel of the recoater mechanism influences measurements. Assessing instrument noise will also be critical.

Powder measurements revealed numerous forms of macroscopic defects which may have been more difficult to identify by a human operator or other sensing methods such as optical imaging. Further, through use of areal surface texture parameters, an algorithmic approach to characterizing defect content over the powder bed was shown to be viable. Further work should examine the contribution of evaluation area size and aspect ratio, globally and locally applied F-operators, and filtering approaches. Additional texture parameters should be examined, and the hybridization of parameters to accomplish more intelligent powder bed defect detection will be explored. Finally, a direct tie between these various powder bed quality measures and as-bult component quality would establish a critical process-structure relationship.

Acknowledgements

The authors acknowledge J. Fox and S. Moylan of NIST for their discussions on metrological characterization. This work was supported by the Department of Energy [DE-EE0008303] and the National Science Foundation [CMMI-1825640].

References

[1] S.K. Everton, M. Hirsch, P. Stravroulakis, R.K. Leach, A.T. Clare, Review of in-situ process monitoring and in-situ metrology for metal additive manufacturing, Materials & Design. 95 (2016) 431–445. https://doi.org/10.1016/j.matdes.2016.01.099.

[2] B.M. Colosimo, S. Cavalli, M. Grasso, A cost model for the economic evaluation of in-situ monitoring tools in metal additive manufacturing, International Journal of Production Economics. 223 (2020) 107532. https://doi.org/10.1016/j.ijpe.2019.107532.

[3] A. du Plessis, I. Yadroitsev, I. Yadroitsava, S.G. Le Roux, X-Ray Microcomputed Tomography in Additive Manufacturing: A Review of the Current Technology and Applications, 3D Printing and Additive Manufacturing. 5 (2018) 227–247. https://doi.org/10.1089/3dp.2018.0060.

[4] Z. Snow, R. Martukanitz, S. Joshi, On the development of powder spreadability metrics and feedstock requirements for powder bed fusion additive manufacturing, Additive Manufacturing. 28 (2019) 78–86. https://doi.org/10.1016/j.addma.2019.04.017.

[5] J. Berez, L. Sheridan, C. Saldaña, Extreme variation in fatigue: Fatigue life prediction and dependence on build volume location in laser powder bed fusion of 17-4 stainless steel, International Journal of Fatigue. 158 (2022) 106737. https://doi.org/10.1016/j.ijfatigue.2022.106737.

[6] A. Soltani-Tehrani, J. Pegues, N. Shamsaei, Fatigue Behavior of Additively Manufactured 17-4 PH Stainless Steel: The Effects of Part Location and Powder Re-use, Additive Manufacturing. (2020). https://doi.org/10.1016/j.addma.2020.101398.

[7] T.P. Moran, D.H. Warner, A. Soltani-Tehrani, N. Shamsaei, N. Phan, Spatial inhomogeneity of build defects across the build plate in laser powder bed fusion, Additive Manufacturing. 47 (2021) 102333. https://doi.org/10.1016/j.addma.2021.102333.

[8] A. Ladewig, G. Schlick, M. Fisser, V. Schulze, U. Glatzel, Influence of the shielding gas flow on the removal of process by-products in the selective laser melting process, Additive Manufacturing. 10 (2016) 1–9. https://doi.org/10.1016/j.addma.2016.01.004.

[9] S. Kleszczynski, ERROR DETECTION IN LASER BEAM MELTING SYSTEMS BY HIGH RESOLUTION IMAGING, (n.d.) 13.

[10] L. Scime, D. Siddel, S. Baird, V. Paquit, Layer-wise anomaly detection and classification for powder bed additive manufacturing processes: A machine-agnostic algorithm for real-time pixel-wise semantic segmentation, Additive Manufacturing. 36 (2020) 101453. https://doi.org/10.1016/j.addma.2020.101453.

[11] L. Scime, J. Beuth, Anomaly detection and classification in a laser powder bed additive manufacturing process using a trained computer vision algorithm, Additive Manufacturing. 19 (2018) 114–126. https://doi.org/10.1016/j.addma.2017.11.009.

[12] D. Schiochet Nasato, H. Briesen, T. Pöschel, Influence of vibrating recoating mechanism for the deposition of powders in additive manufacturing: Discrete element simulations of polyamide 12, Additive Manufacturing. 48 (2021) 102248. https://doi.org/10.1016/j.addma.2021.102248.

[13] J.A. Slotwinski, E.J. Garboczi, Metrology Needs for Metal Additive Manufacturing Powders, JOM. 67 (2015) 6. https://doi.org/10.1007/s11837-014-1290-7.

[14] A.T. Sutton, C.S. Kriewall, M.C. Leu, J.W. Newkirk, Powders for Additive Manufacturing Processes: Characterization Techniques and Effects on Part Properties, (n.d.) 27.

[15] I.E. Anderson, E.M.H. White, R. Dehoff, Feedstock powder processing research needs for additive manufacturing development, Current Opinion in Solid State and Materials Science. 22 (2018) 8–15. https://doi.org/10.1016/j.cossms.2018.01.002.
[16] J. Clayton, D. Millington-Smith, B. Armstrong, The Application of Powder Rheology in Additive Manufacturing, JOM. 67 (2015) 544–548. https://doi.org/10.1007/s11837-015-1293-z.
[17] G. Jacob, C.U. Brown, M.A. Donmez, S.S. Watson, J. Slotwinski, Effects of powder recycling on stainless steel powder and built material properties in metal powder bed fusion processes, National Institute of Standards and Technology, Gaithersburg, MD, 2017. https://doi.org/10.6028/NIST.AMS.100-6.
[18] P.E. Carrion, A. Soltani-Tehrani, N. Phan, N. Shamsaei, Powder Recycling Effects on the Tensile and Fatigue Behavior of Additively Manufactured Ti-6Al-4V Parts, JOM. 71 (2019) 963–973. https://doi.org/10.1007/s11837-018-3248-7.
[19] F. Ahmed, U. Ali, D. Sarker, E. Marzbanrad, K. Choi, Y. Mahmoodkhani, E. Toyserkani, Study of powder recycling and its effect on printed parts during laser powder-bed fusion of 17-4 PH stainless steel, Journal of Materials Processing Technology. 278 (2020) 116522. https://doi.org/10.1016/j.jmatprotec.2019.116522.
[20] J. Berez, C. Saldana, Fatigue of laser powder bed fusion processed 17-4 stainless steel using prior process exposed powder feedstock, Journal of Manufacturing Processes. 71 (2021) 515–527. https://doi.org/10.1016/j.jmapro.2021.09.045.
[21] M.J. Heiden, L.A. Deibler, J.M. Rodelas, J.R. Koepke, D.J. Tung, D.J. Saiz, B.H. Jared, Evolution of 316L stainless steel feedstock due to laser powder bed fusion process, Additive Manufacturing. 25 (2019) 84–103. https://doi.org/10.1016/j.addma.2018.10.019.
[22] A. Strondl, O. Lyckfeldt, H. Brodin, U. Ackelid, Characterization and Control of Powder Properties for Additive Manufacturing, JOM. 67 (2015) 549–554. https://doi.org/10.1007/s11837-015-1304-0.
[23] A.B. Anwar, Q.-C. Pham, Study of the spatter distribution on the powder bed during selective laser melting, Additive Manufacturing. 22 (2018) 86–97. https://doi.org/10.1016/j.addma.2018.04.036.
[24] R.W. Penny, P.M. Praegla, M. Ochsenius, D. Oropeza, C. Meier, W.A. Wall, A.J. Hart, Spatial Mapping of Powder Layer Density for Metal Additive Manufacturing via X-ray Microscopy, ArXiv:2103.13421 [Physics]. (2021). http://arxiv.org/abs/2103.13421 (accessed April 16, 2021).
[25] B. Zhang, J. Ziegert, F. Farahi, A. Davies, In situ surface topography of laser powder bed fusion using fringe projection, Additive Manufacturing. 12 (2016) 100–107. https://doi.org/10.1016/j.addma.2016.08.001.
[26] H. Zhang, C.K.P. Vallabh, Y. Xiong, X. Zhao, A systematic study and framework of fringe projection profilometry with improved measurement performance for in-situ LPBF process monitoring, Measurement. 191 (2022) 110796. https://doi.org/10.1016/j.measurement.2022.110796.
[27] F. Sillani, R. Schiegg, M. Schmid, E. MacDonald, K. Wegener, Powder Surface Roughness as Proxy for Bed Density in Powder Bed Fusion of Polymers, Polymers. 14 (2021) 81. https://doi.org/10.3390/polym14010081.
[28] C. Barrett, E. MacDonald, B. Conner, F. Persi, Micron-Level Layer-Wise Surface Profilometry to Detect Porosity Defects in Powder Bed Fusion of Inconel 718, JOM. 70 (2018) 1844–1852. https://doi.org/10.1007/s11837-018-3025-7.